

# BAND-LIMITED MAXIMIZERS FOR A FOURIER EXTENSION INEQUALITY ON THE CIRCLE, II

JAMES BARKER, CHRISTOPH THIELE, AND PAVEL ZORIN-KRANICH

ABSTRACT. Among the class of functions on the circle with Fourier modes up to degree 120, constant functions are the unique real-valued maximizers for the endpoint Tomas–Stein inequality.

## 1. INTRODUCTION

This article continues the investigation in [OTZ19] of extremizers of the classical Tomas–Stein [Tom75] Fourier extension inequality on the circle in classes of band limited functions. We improve the main theorem in [OTZ19], which concerns functions with Fourier modes up to degree 30, towards degree  $N = 120$ .

**Theorem 1.** *Let  $f \in L^2(\mathbb{S}^1)$  be real-valued. Assume that  $\widehat{f}_n = 0$  for all  $n > 120$ . Then*

$$\Phi(f) \leq \Phi(\mathbf{1}),$$

*with equality if and only if  $f$  is constant.*

Here,  $\mathbb{S}^1$  is the unit circle in the complex plane, and  $\widehat{f}_n$  are the coefficients in the Fourier series

$$f(\omega) = \sum_{n \in \mathbb{Z}} \widehat{f}_n \omega^n.$$

The Tomas–Stein functional

$$\Phi(f) := \left\| \widehat{f\sigma} \right\|_{L^6(\mathbb{R}^2)}^6 \|f\|_{L^2(\mathbb{S}^1)}^{-6}$$

is the sixth power of the norm quotient for the Fourier extension map

$$\widehat{f\sigma}(x) := \int_{\mathbb{S}^1} f(\omega) e^{-ix \cdot \omega} d\sigma_\omega, \quad (x \in \mathbb{R}^2),$$

where we identify the complex plane with the Euclidean plane  $\mathbb{R}^2$  when we take the dot product  $x \cdot \omega$ , and  $\sigma$  is the arclength measure on the circle. The constant function  $\mathbf{1}$  is conjectured to extremize the functional  $\Phi$  among all functions in  $L^2(\mathbb{S}^1)$ .

We refer to [Car+17],[OTZ19], and [FO17] for further background on the sharp Fourier restriction and extension problems. In particular, it is known that real-valued maximizers of the functional  $\Phi$  do not change sign and are antipodally symmetric. Hence, it suffices to show the variant of Theorem 1 for non-negative and antipodally symmetric functions as in [OTZ19].

Since  $f$  in Theorem 1 is assumed to be real-valued, we have  $\widehat{f}_n = \widehat{f}_{-n}$ , so that the Fourier modes vanish for  $|n| > 120$ . Theorem 1 thus concerns finite

set of Fourier modes and turns the extremizing problem into a finite dimensional problem. This makes it accessible to numerical computation. As in [OTZ19], the theorem is reduced to demonstrating positive semi-definiteness of each of the  $3N/2 + 1$  matrices

$$(1) \quad (Q_{\mathbf{m},\mathbf{n}})_{\mathbf{m},\mathbf{n} \in X_D}$$

with  $0 \leq D \leq 3N$  an even number,

$$X_D = \left\{ (m_1, m_2, m_3) \in (2\mathbb{Z})^3 \setminus \{(0,0,0)\} \mid \begin{array}{l} m_1+m_2+m_3=D, \\ |m_1|, |m_2|, |m_3| \leq N, \\ m_1 \leq m_2 \leq m_3 \end{array} \right\},$$

and, writing  $S_3$  for the group of permutations of three elements and

$$\mathbf{n}_\sigma = (n_{\sigma(1)}, n_{\sigma(2)}, n_{\sigma(3)}), \quad \sigma \in S_3,$$

we set

$$\begin{aligned} Q_{\mathbf{m},\mathbf{n}} &:= \frac{1}{6} \sum_{\sigma \in S_3} (R_{\mathbf{m},\mathbf{n}_\sigma} - L_{\mathbf{m},\mathbf{n}_\sigma}), \\ L_{\mathbf{m},\mathbf{n}} &:= 2I_{\mathbf{m},-\mathbf{n}} + \sum_{\sigma \in S_3} I_{\mathbf{m},-\mathbf{n}+(1,-1,0)_\sigma}, \\ R_{\mathbf{m},\mathbf{n}} &:= 2I_{\mathbf{m}-\mathbf{n},(0,0,0)} + \sum_{\sigma \in S_3} I_{\mathbf{m}-\mathbf{n},(1,-1,0)_\sigma}, \\ I_{\mathbf{k}} &:= \int_0^\infty \prod_{j=1}^6 J_{k_j}(r) r \, dr, \end{aligned}$$

where the Bessel function  $J_k$  is defined by

$$\int_{\mathbb{S}^1} \omega^k e^{-ix \cdot \omega} \, d\sigma_\omega = 2\pi (-i)^k J_k(|x|)(x/|x|)^k.$$

Note that in the formulas for  $L_{\mathbf{m},\mathbf{n}}$  and  $R_{\mathbf{m},\mathbf{n}}$  given in [OTZ19],  $\mathbf{n}$  should be replaced by  $-\mathbf{n}$  on the right-hand side. This error is corrected here.

The main computational task in the proof of the theorem is the numerical approximation of the various integrals  $I_{\mathbf{k}}$ . The number of such integrals increases as the fifth power of  $N$ ; approximately  $2.1 \times 10^5$  distinct integrals (up to sign and permutation of  $\mathbf{k}$ ) must be calculated for the  $N = 30$  case, increasing to approximately  $1.6 \times 10^8$  for the  $N = 120$  case. In Section 2, we describe carefully the numerical scheme used to approximate each  $I_{\mathbf{k}}$  and estimate the associated error. This scheme is an improved version of the scheme given in [OTZ19], requiring fewer arithmetic operations per integral. We also discuss the adjustment of the parameters in the scheme for arbitrary  $N$ .

Due to the high level of precision required, the various calculations used in the proof were performed using arbitrary-precision arithmetic as implemented in the Arb numerical library [Joh17]; when used carefully, such arithmetic provides rigorous error bounds for the output of calculations. The calculation code was written in C++, employing hybrid parallelization through the use of both OpenMP and MPI. Computations were performed in parallel using 94 nodes of a modern compute cluster, requiring approximately 30 hours of wall time. Weights and points used for Gauss-Legendre quadrature were calculated using Mathematica [W19] to high precision and imported into the main calculation code by hand. The complete code used

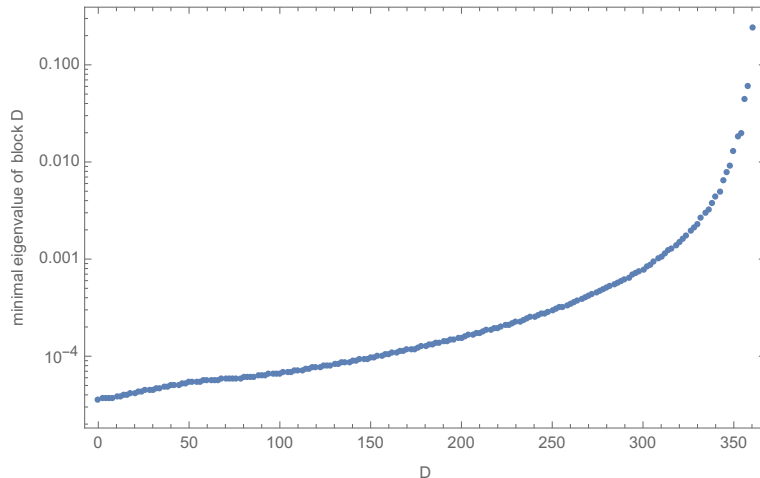


FIGURE 1. Approximated smallest eigenvalue for each matrix in 1 with  $0 \leq D \leq 360$ ,  $N = 120$ .

to generate the results relied upon in the proof is included in the supporting information of this paper, along with the raw output of the calculation. Some supporting information (plots, etc.) outside the scope of the main proof was calculated by post-processing the calculated integrals  $I_{\mathbf{k}}$  using standard numerical software, as the precision requirements are in context less stringent.

In Section 3, we describe the results of these computations, give an assessment of the eigenvalues, and discuss various plots of matrix entries and eigenfunctions. The quality of the experimentally-obtained information about the matrices in (1) and their eigenvalues and eigenfunctions has substantially improved compared to the computations in [OTZ19]. Phenomena are seen with much better resolution and allow further investigation. In particular, we obtain positivity of all eigenvalues in question, as shown to sufficient accuracy in Figure 1, which implies Theorem 1 by the reductions described in [OTZ19].

Figure 1 shows that  $D = 0$  has the smallest eigenvalue among the matrices in 1 for  $N = 120$ . It is cheap to conjecture that the analogous statement holds for arbitrarily large  $N$ . If in addition one conjectures an asymptotic behaviour of the smallest eigenvalue of the matrix  $D = 0$  as suggested by Figure 2, one can conclude from these conjectures the analogue to Theorem 1 for arbitrarily large  $N$ , and with it the general conjecture about constant functions maximizing the Tomas–Stein functional in  $L^2(\mathbb{S}^1)$ .

## 2. NUMERICAL ESTIMATION OF $I_{\mathbf{k}}$ AND ERROR BOUNDS

As in [OTZ19], we approximate integrals  $I_{\mathbf{k}}$  by quantities  $\tilde{I}_{\mathbf{k}}$  defined by approximating schemes. We split

$$(2) \quad I_{\mathbf{k}} = I_{\mathbf{k}}^{0,S} + I_{\mathbf{k}}^{S,T} + I_{\mathbf{k}}^{T,\infty}$$

$$= \int_0^S \prod_{j=1}^6 J_{k_j}(r)r \, dr + \int_S^T \prod_{j=1}^6 J_{k_j}(r)r \, dr + \int_T^\infty \prod_{j=1}^6 J_{k_j}(r)r \, dr,$$

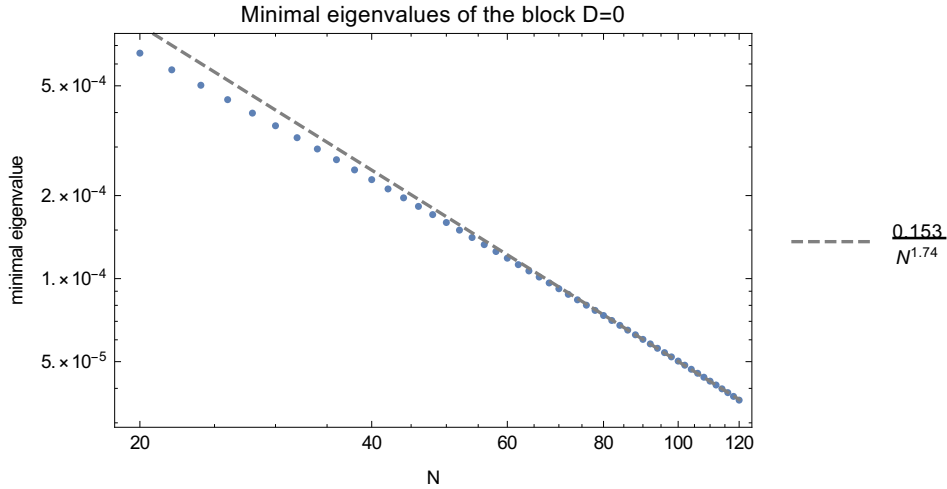


FIGURE 2. Approximated smallest eigenvalue for the  $D = 0$  matrix in (1) with  $20 \leq N \leq 120$ .

and correspondingly combine

$$\tilde{I}_{\mathbf{k}} = \tilde{I}_{\mathbf{k}}^{0,S} + \tilde{I}_{\mathbf{k}}^{S,T} + \tilde{I}_{\mathbf{k}}^{T,\infty},$$

where the first two terms are quadrature rules with different parameters approximating the corresponding compact integrals in (2), and the third term is an exact integral over an approximation to the integrand using asymptotic expansion. As opposed to [OTZ19], we use Gauss-Legendre quadrature instead of Newton-Cotes quadrature on the first two pieces, and we use more terms of the asymptotic expansion on the third integral. The cutoffs  $S$  and  $T$  should be chosen well for numerical speed and accuracy. Our discussion of the error bounds requires  $S \geq N^{3/2} \ln(N) + 1$  and  $T > 10N^2$ . For  $N = 120$ , in accordance with these conditions, we choose  $S = 6,000$  and  $T = 150,000$ .

### 2.1. Gauss-Legendre quadrature on the intervals $[0, S]$ and $[S, T]$ .

We cut each of the intervals  $[0, S]$  and  $[S, T]$  into small intervals of constant length and use Gauss-Legendre quadrature with  $n = 12$  points on each of these small intervals. We will estimate the error of the quadrature using Lemma 3 below. We first quickly review the theory behind this lemma.

On  $L^2([-1,1])$ , the even or odd real monic polynomial

$$(3) \quad \frac{n!}{(2n)!} \partial^n (x^2 - 1)^n =: \prod_{i=1}^n (x - x_i) =: p_n(x)$$

is orthogonal to all polynomials of lower degree. This is seen by  $n$ -fold partial integration, with boundary terms vanishing due to the structure of  $p_n$ . The zeroes  $x_1, \dots, x_n$  are distinct and contained in  $(-1,1)$ , or else there was a lower degree polynomial with the same sign as  $p_n$  on  $[-1,1]$ , contradicting orthogonality. The linear combination  $x p_n - p_{n+1}$  has degree at most  $n$  and is orthogonal to all polynomials  $p_k$  with  $k < n - 1$ . By parity consideration, it is a multiple of  $p_{n-1}$  with factor determined by examination of the highest order coefficient:

$$x p_n - p_{n+1} =$$

$$\left[ \frac{-n^2(n-1)}{(2n)(2n-1)} - \frac{-(n+1)^2n}{(2n+2)(2n+1)} \right] p_{n-1} = \frac{n^2}{(2n+1)(2n-1)} p_{n-1}.$$

Pairing with  $p_{n-1}$ , using orthogonality relations, identifying the  $n$ -th factor of the Wallis product, and solving the recursion yields

$$\int_{-1}^1 p_n^2(x) dx = \frac{1}{4} \frac{(2n)^2}{(2n-1)(2n+1)} \int_{-1}^1 p_{n-1}^2(x) dx \leq 2^{-2n} \pi.$$

**Lemma 2** (Gauss-Legendre quadrature). *There are weights  $w_i$  such that, for every function  $f$  that is  $2n$  times continuously differentiable on  $[-1,1]$ , we have*

$$(4) \quad \left| \int_{-1}^1 f(y) dy - \sum_{i=1}^n w_i f(x_i) \right| \leq \pi 2^{-2n} \sup_{\xi \in [-1,1]} \frac{|f^{(2n)}(\xi)|}{(2n)!}.$$

*Proof.* By regularity of the Vandermonde determinant, there are weights  $w_i$  such that the left-hand-side of (4) vanishes if  $f$  is a polynomial of degree at most  $n-1$ . The left-hand-side also vanishes evidently for all polynomials of the form  $x^k p_n$  with  $k \leq n-1$ , and thus for all polynomials of degree at most  $2n-1$ . For arbitrary  $f$  as in the lemma, let  $h$  be the polynomial of degree  $< 2n$  such that  $f-h$  vanishes of second order at all points  $x_i$ . Then the function  $k = (f-h)p_n^{-2}$  is continuous. We estimate the left-hand-side of (4) as:

$$\int_{-1}^1 (f-h)(y) dy = \int_{-1}^1 k(y) p_n(y)^2 dy \leq |k(x)| \int_{-1}^1 p_n(y)^2 dy \leq \pi 2^{-2n} |k(x)|$$

for some  $x \in [-1,1]$ . By Rolle's theorem, there is a  $\xi \in [-1,1]$  with

$$0 = \partial_\xi^{2n} (f-h-k(x)p_n^2)(\xi) = f^{(2n)}(\xi) - k(x)(2n)! \quad \square$$

**Lemma 3.** *Assume  $f$  is analytic on the union of balls of radius 1 about each of the points of the interval  $[a,b]$  and bounded by  $F$  on this union. Then*

$$\left| \int_a^b f(x) dx - \sum_{i=1}^n w_i \frac{b-a}{2} f\left(\frac{a+b}{2} + \frac{b-a}{2} x_i\right) \right| \leq \pi 2^{-2n} \left(\frac{|b-a|}{2}\right)^{2n+1} F.$$

*Proof.* This follows by translation and dilation of  $f$  from the case  $[a,b] = [-1,1]$  with balls of radius 1 replaced by balls of radius  $2/|b-a|$ . The estimate in case  $[-1,1]$  follows from Lemma 4 when estimating  $\frac{f^{(2n)}(\xi)}{2n!}$  with Cauchy's integral formula as an average of the analytic function  $f$  over the circle of radius  $2/|b-a|$  about the point  $\xi$ .  $\square$

On the interval  $[0, S]$ , we use the bound

$$|J_n(z)| \leq e^{|\Im(z)|}$$

on the strip  $\Im(z) \leq 1$ , obtained as reviewed in Section 2 of [OT15] from the integral representation

$$J_n(z) = \frac{1}{2\pi} \int_0^{2\pi} e^{iz \sin(\theta)} e^{in\theta} d\theta.$$

Hence, the function

$$(5) \quad f(z) = z \prod_{i=1}^6 J_{n_i}(z)$$

is bounded in absolute value by  $|z|e^6$  on this strip. Cutting the interval  $[0, S]$  into  $K$  intervals of length  $2d = S/K < 1$  and using Gauss-Legendre quadrature as in Lemma (3) on each interval gives

$$\begin{aligned} |I_{\mathbf{k}}^{0,S} - \tilde{I}_{\mathbf{k}}^{0,S}| &= \left| \int_0^S f(z) dz - \sum_{j=0}^{K-1} d \sum_{i=1}^n w_i f(d(2j+1) + dx_i) \right| \\ &\leq \pi 2^{-2n} d^{2n+1} e^6 \sum_{j=0}^{K-1} (2d(j+1) + 1) \leq \pi 2^{-2n} d^{2n} e^6 \int_0^S (x+2) dx \end{aligned}$$

$$(6) \quad \pi 2^{-2n} d^{2n} e^6 (S+2)^2 \leq 0.0000756 \times (S+2)^2 d^{24} \leq 0.1 \times 10^{-10}.$$

Here we have used  $n = 12$  in the penultimate and  $S = 6,000$  and  $d = 0.25$  in the ultimate inequality. Note that this estimate does not depend on particular assumptions on  $S$ , and our parameters lead to an algorithm with 144,000 evaluations of the integrand.

On the interval  $[S, T]$ , we recall from [OT15, Section 2] the following representation for  $J_n$ , which arises through the change of variables  $t = \cos(\theta)$  from the Poisson integral:

$$J_n(z) = \frac{(z/2)^n}{\Gamma(n+1/2)\Gamma(1/2)} \int_{-1}^1 \cos(zt)(1-t^2)^{n-1/2} dt.$$

We split  $J_n = \frac{1}{2}(J_n^+ + J_n^-)$ , where  $J_n^+(\bar{z}) = \overline{J_n^-(z)}$  and

$$J_n^+(z) = \frac{(z/2)^n}{\Gamma(n+1/2)\Gamma(1/2)} \int_{-1}^1 e^{izt}(1-t^2)^{n-1/2} dt.$$

A change of the contour integral leads to

$$(7) \quad J_n^+(z) = \frac{(2\pi z)^{-1/2}}{\Gamma(\nu+1)} \int_0^\infty e^{-u} u^\nu \left[ e^{-i\omega} \left(1 - \frac{i u}{2z}\right)^\nu + e^{i\omega} \left(1 + \frac{i u}{2z}\right)^\nu \right] du$$

with the abbreviations

$$\begin{aligned} \nu &:= n - 1/2, \\ \omega &:= z - \frac{\pi}{4} - \frac{n\pi}{2}. \end{aligned}$$

We split further  $J_n^+ = \frac{1}{2}(J_n^{++} + J_n^{+-})$  with  $J_n^{+-}(\bar{z}) = \overline{J_n^{++}(z)}$  and

$$(8) \quad J_n^{++}(z) = \left(\frac{2}{\pi z}\right)^{1/2} \frac{e^{i\omega}}{\Gamma(\nu+1)} \int_0^\infty e^{-u} u^\nu \left(1 + \frac{i u}{2z}\right)^\nu du.$$

**Lemma 4.** *Assume  $N \geq 20$  and  $0 \leq n \leq N$ . Assume  $|\Re(z)| > N^{\frac{3}{2}} \ln N$  and  $|\Im(z)| \leq 1$ . Then*

$$|J_n^{++}(z)| \leq 3.36|z|^{-1/2}.$$

*The analogous estimate holds for  $J_n^{+-}$ ,  $J_n^+$ ,  $J_n^-$ , and  $J_n$ .*

*Proof.* We first estimate the part of the integral in (8) from 0 to  $2N \ln N$ . We estimate in this range

$$1 + \frac{iu}{2z} = 1 - \frac{u\Im(z)}{2|z|^2} + i\frac{u\Re(z)}{2|z|^2}$$

$$\frac{1}{2} \leq \left|1 + \frac{iu}{2z}\right| \leq \sqrt{\left(1 + \frac{1}{N^2 \ln(N)}\right)^2 + \frac{1}{N}} \leq 1 + \frac{1}{N},$$

where the lower bound by  $\frac{1}{2}$  will only be used if  $\nu$  is negative, that is  $\nu = -1/2$ . We obtain

$$\left| \int_0^{2N \ln N} e^{-u} u^\nu \left(1 + \frac{iu}{2z}\right)^\nu du \right| \leq e \int_0^\infty e^{-u} u^\nu du = e\Gamma(\nu + 1).$$

Turning to the part of the integral in (8) from  $2N \ln(N)$  to  $\infty$ , we estimate

$$\left|1 \pm \frac{iu}{2z}\right|^\nu \leq \left(\frac{u}{N}\right)^{\nu+2}.$$

Hence we have

$$\begin{aligned} \left| \int_{2N \ln N}^\infty e^{-u} u^\nu \left(1 + \frac{iu}{2z}\right)^\nu du \right| &\leq e^{-N \ln(N)} \int_0^\infty e^{-u/2} u^\nu \left(\frac{u}{N}\right)^{\nu+2} du \\ &= N^{-N-\nu-2} 2^{2\nu+3} \Gamma(2\nu + 3) \leq \frac{1}{100} \Gamma(\nu + 1). \end{aligned}$$

With  $|e^{i\omega}| \leq \cosh(|\Im z|) \leq \cosh(1)$  it follows that

$$|J_n^+(z)| \leq \left(\frac{2}{\pi|z|}\right)^{1/2} \cosh(1) \left(\frac{1}{100} + e\right) \leq 3.36|z|^{-1/2}.$$

The analogous estimates for the other variants of Bessel's function are clear.  $\square$

With Lemma 4, we estimate the function (5) on the strip  $\Im(z) \leq 1$  and  $\Re(z) \geq N^{\frac{3}{2}} \ln(N)$  in absolute value by (3.36)<sup>6</sup> $|z|^{-2}$ . Cutting the interval  $[S, T]$  into  $K$  intervals of length  $2d = (T - S)/K < 1$  and using Gauss-Legendre quadrature as in Lemma (3) on each interval, we obtain

$$\begin{aligned} |I_{\mathbf{k}}^{S,T} - \tilde{I}_{\mathbf{k}}^{S,T}| &= \left| \int_S^T f(z) dz - \sum_{j=0}^{K-1} d \sum_{i=1}^n w_i f(S + d(2j+1) + dx_i) \right| \\ &\leq \frac{\pi}{2^{2n}} d^{2n+1} (3.36)^6 \sum_{j=0}^{K-1} (S + 2dj - 1)^{-2} \leq \frac{\pi}{2^{2n}} d^{2n} (3.36)^6 \int_S^T (x-2)^{-2} dx \end{aligned}$$

$$(9) \leq \pi 2^{-2n} d^{2n} (3.36)^6 (S-2)^{-1} \leq 0.00027 \times (S-2)^{-1} d^{24} \leq 2.2 \times 10^{-10}.$$

Here we used  $n = 12$  in the penultimate and  $S = 6,000$  and  $d = 0.8$  in the ultimate inequality. The use of Lemma 4 here requires  $S \geq N^{3/2} \ln(N) + 1$ , which is satisfied with  $N = 120$  and  $S = 6,000$ . Assuming  $T = 150,000$ , this amounts to 1,080,000 evaluations of the integrand.

**2.2. Asymptotic approximation on the interval  $[T, \infty)$ .** We present a precise error bound for the classical asymptotic expansion of order four of Bessel functions, a slight refinement of the corresponding discussion in Section 2 of [OT15].

**Lemma 5.** *Assume  $N \geq 20$  and  $n \leq N$ . Assume  $z$  is real and  $z > 2N^{\frac{3}{2}} \ln(N)$ . Then*

$$(10) \quad \left(\frac{\pi z}{2}\right)^{\frac{1}{2}} J_n^{++}(z) e^{-i\omega} = 1 + i \frac{\Gamma(\nu+2)}{2\Gamma(\nu)z} - \frac{\Gamma(\nu+3)}{8\Gamma(\nu-1)z^2} - i \frac{\Gamma(\nu+4)}{48\Gamma(\nu-2)z^3} + R$$

with

$$|R| \leq 0.0043 \frac{N^8}{z^4}.$$

*Proof.* Recalling (8), we see

$$(11) \quad \left(\frac{\pi z}{2}\right)^{\frac{1}{2}} J_n^{++}(z) e^{-i\omega} = \frac{1}{\Gamma(\nu+1)} \int_0^\infty e^{-u} u^\nu \left(1 + \frac{i u}{2z}\right)^\nu du.$$

We expand  $(1 + ix)^\nu$  for real  $0 \leq x$  with Taylor's theorem into

$$(1 + ix)^\nu = 1 + i\nu x - \frac{1}{2}\nu(\nu-1)x^2 - \frac{1}{6}i\nu(\nu-1)(\nu-2)x^3 + r$$

Where

$$\begin{aligned} |r| &= \left| \int_0^x \frac{1}{6} \nu(\nu-1)(\nu-2)(\nu-3)(x-t)^3 (1+it)^{\nu-4} dt \right| \\ &\leq \frac{1}{24} \nu(\nu-1)(\nu-2)(\nu-3) x^4 (1+x^2)^{\frac{1}{2} \max(\nu-4, 0)}. \end{aligned}$$

Thus the right hand side of (11) becomes (10) with

$$|R| \leq \int_0^\infty e^{-u} u^\nu |r(u)| du$$

and  $r(u)$  similar to above with  $x$  replaced by  $u/2z$ . We cut the integral at  $u = 4N \ln(N)$ . For  $u \leq 4N \ln(N)$  we have

$$|r(u)| \leq \frac{\nu(\nu-1)(\nu-2)(\nu-3)u^4}{384z^4} \left(1 + \frac{1}{N}\right)^{\frac{N}{2}}$$

and thus

$$\frac{1}{\Gamma(\nu+1)} \int_0^{4N \ln(N)} e^u u^\nu r(u) du \leq e^{1/2} \frac{\Gamma(\nu+5)}{384\Gamma(\nu-3)z^4} \leq \frac{e^{1/2} N^8}{384z^4}.$$

For  $u \geq 4N \ln(N)$  we have

$$\begin{aligned} |r(u)| &\leq \frac{\nu(\nu-1)(\nu-2)(\nu-3)u^4}{6(2z)^4} \left(\frac{u}{N}\right)^{N/2} \\ &\frac{1}{\Gamma(\nu+1)} \int_{4N \ln(N)}^\infty e^{-u} u^\nu r(u) du \\ &\leq \frac{1}{384z^4 \Gamma(\nu-3)} \int_0^\infty e^{-u/2} e^{-2N \ln(N)} u^{\nu+4} \left(\frac{u}{N}\right)^{N/2} du \end{aligned}$$



$$\leq \frac{1}{96z^4\Gamma(\nu-3)} \frac{2^{\nu+5+N/2}}{N^{2N+N/2}} \Gamma(\nu+5+N/2) \leq z^{-4}.$$

Adding the estimates for the two pieces of the integral gives the bound claimed in the lemma.  $\square$

With the above lemma, we obtain for  $J_n^+$  in the range of  $n$  and  $z$  discussed in the lemma:

$$(12) \quad \left(\frac{\pi z}{2}\right)^{\frac{1}{2}} J_n^+(z) = a + bz^{-1} + cz^{-2} + dz^{-3} + R$$

with

$$\begin{aligned} a &= \cos(\omega) \\ b &= -\sin(\omega) \frac{1}{2} \left(n^2 - \frac{1}{4}\right) \\ c &= -\cos(\omega) \frac{1}{8} \left(n^2 - \frac{1}{4}\right) \left(n^2 - \frac{9}{4}\right) \\ d &= +\sin(\omega) \frac{1}{48} \left(n^2 - \frac{1}{4}\right) \left(n^2 - \frac{9}{4}\right) \left(n^2 - \frac{25}{4}\right) \end{aligned}$$

and where  $R$  satisfies the same bounds as in the lemma. The analogous identity holds for  $J_n$  since it coincides with  $J_n^+$  on the real line. Now we consider six indices  $n_j$  and corresponding  $\omega_j$  and obtain for real  $z$

$$\left(\frac{\pi}{2}\right)^3 \prod_{j=1}^6 J_{n_j}(z)z = Az^{-2} + Bz^{-3} + Cz^{-4} + Q$$

with

$$A = \cos(\omega_1) \cos(\omega_2) \cos(\omega_3) \cos(\omega_4) \cos(\omega_5) \cos(\omega_6),$$

$$\begin{aligned} B &= -\frac{n_1^2 - 1/4}{2} \sin(\omega_1) \cos(\omega_2) \cos(\omega_3) \cos(\omega_4) \cos(\omega_5) \cos(\omega_6) \\ &\quad - \frac{n_2^2 - 1/4}{2} \cos(\omega_1) \sin(\omega_2) \cos(\omega_3) \cos(\omega_4) \cos(\omega_5) \cos(\omega_6) \\ &\quad - \frac{n_3^2 - 1/4}{2} \cos(\omega_1) \cos(\omega_2) \sin(\omega_3) \cos(\omega_4) \cos(\omega_5) \cos(\omega_6) \\ &\quad - \frac{n_4^2 - 1/4}{2} \cos(\omega_1) \cos(\omega_2) \cos(\omega_3) \sin(\omega_4) \cos(\omega_5) \cos(\omega_6) \\ &\quad - \frac{n_5^2 - 1/4}{2} \cos(\omega_1) \cos(\omega_2) \cos(\omega_3) \cos(\omega_4) \sin(\omega_5) \cos(\omega_6) \\ &\quad - \frac{n_6^2 - 1/4}{2} \cos(\omega_1) \cos(\omega_2) \cos(\omega_3) \cos(\omega_4) \cos(\omega_5) \sin(\omega_6), \end{aligned}$$

$$\begin{aligned} C &= +\frac{(n_1^2 - 1/4)(n_2^2 - 1/4)}{4} \sin(\omega_1) \sin(\omega_2) \cos(\omega_3) \cos(\omega_4) \cos(\omega_5) \cos(\omega_6) \\ &\quad +\frac{(n_1^2 - 1/4)(n_3^2 - 1/4)}{4} \sin(\omega_1) \cos(\omega_2) \sin(\omega_3) \cos(\omega_4) \cos(\omega_5) \cos(\omega_6) \\ &\quad +\frac{(n_1^2 - 1/4)(n_4^2 - 1/4)}{4} \sin(\omega_1) \cos(\omega_2) \cos(\omega_3) \sin(\omega_4) \cos(\omega_5) \cos(\omega_6) \\ &\quad +\frac{(n_1^2 - 1/4)(n_5^2 - 1/4)}{4} \sin(\omega_1) \cos(\omega_2) \cos(\omega_3) \cos(\omega_4) \sin(\omega_5) \cos(\omega_6) \end{aligned}$$

$$\begin{aligned}
& + \frac{(n_1^2 - 1/4)(n_6^2 - 1/4)}{4} \sin(\omega_1) \cos(\omega_2) \cos(\omega_3) \cos(\omega_4) \cos(\omega_5) \sin(\omega_6) \\
& + \frac{(n_2^2 - 1/4)(n_3^2 - 1/4)}{4} \cos(\omega_1) \sin(\omega_2) \sin(\omega_3) \cos(\omega_4) \cos(\omega_5) \cos(\omega_6) \\
& + \frac{(n_2^2 - 1/4)(n_4^2 - 1/4)}{4} \cos(\omega_1) \sin(\omega_2) \cos(\omega_3) \sin(\omega_4) \cos(\omega_5) \cos(\omega_6) \\
& + \frac{(n_2^2 - 1/4)(n_5^2 - 1/4)}{4} \cos(\omega_1) \sin(\omega_2) \cos(\omega_3) \cos(\omega_4) \sin(\omega_5) \cos(\omega_6) \\
& + \frac{(n_2^2 - 1/4)(n_6^2 - 1/4)}{4} \cos(\omega_1) \sin(\omega_2) \cos(\omega_3) \cos(\omega_4) \cos(\omega_5) \sin(\omega_6) \\
& + \frac{(n_3^2 - 1/4)(n_4^2 - 1/4)}{4} \cos(\omega_1) \cos(\omega_2) \sin(\omega_3) \sin(\omega_4) \cos(\omega_5) \cos(\omega_6) \\
& + \frac{(n_3^2 - 1/4)(n_5^2 - 1/4)}{4} \cos(\omega_1) \cos(\omega_2) \sin(\omega_3) \cos(\omega_4) \sin(\omega_5) \cos(\omega_6) \\
& + \frac{(n_3^2 - 1/4)(n_6^2 - 1/4)}{4} \cos(\omega_1) \cos(\omega_2) \sin(\omega_3) \cos(\omega_4) \cos(\omega_5) \sin(\omega_6) \\
& + \frac{(n_4^2 - 1/4)(n_5^2 - 1/4)}{4} \cos(\omega_1) \cos(\omega_2) \cos(\omega_3) \sin(\omega_4) \sin(\omega_5) \cos(\omega_6) \\
& + \frac{(n_4^2 - 1/4)(n_6^2 - 1/4)}{4} \cos(\omega_1) \cos(\omega_2) \cos(\omega_3) \sin(\omega_4) \cos(\omega_5) \sin(\omega_6) \\
& + \frac{(n_5^2 - 1/4)(n_6^2 - 1/4)}{4} \cos(\omega_1) \cos(\omega_2) \cos(\omega_3) \cos(\omega_4) \sin(\omega_5) \sin(\omega_6) \\
& - \frac{\left[ \sum_{j=1}^6 (n_j^2 - 1/4)(n_j^2 - 9/4) \right]}{8} \cos(\omega_1) \cos(\omega_2) \cos(\omega_3) \cos(\omega_4) \cos(\omega_5) \cos(\omega_6).
\end{aligned}$$

The remainder term  $Q$  we estimate from above. For this we collect terms of order  $z^{-5}$ ,  $z^{-6}$ ,  $z^{-7}$ ,  $z^{-8}$  and higher order separately.

We begin with a remark on integrals of type

$$\int_T^\infty \prod_{j=1}^6 \phi_j(\omega_j) z^{-5}$$

where an odd number of functions  $\phi_j$  are the cosine function and an odd number of  $\phi_j$  are the sine function.

If a function is odd in the variable  $z$  about the point  $\frac{\pi}{4}$  then we call it of parity  $-1$ , and if it is even we call it of parity  $1$ . The function

$$\sin(\omega_j) = \sin\left(z - \frac{\pi}{4} - \frac{n\pi}{2}\right)$$

has parity  $-(-1)^n$  about the point  $\frac{\pi}{4}$ , while the function

$$\cos(\omega_j) = \cos\left(z - \frac{\pi}{4} - \frac{n\pi}{2}\right)$$

has parity  $(-1)^n$ . A product of six such functions with  $\sum_{j=1}^6 n_j$  even and an involving an odd number of sine function is therefore odd about the point

$\pi/4$ . This means it integrates to zero about each period of the periodic function. Hence by partial integration

$$\begin{aligned} & \left| \int_T^\infty \prod_{j=1}^6 \phi_j(\omega_j) z^{-5} dz \right| \leq \\ & \left| \int_T^\infty \partial^{-1} \left[ \prod_{j=1}^6 \phi_j(\omega_j) \right] 5z^{-6} dz \right| + T^{-5} \\ & \leq (\pi + 1)T^{-5}, \end{aligned}$$

where we used that the function  $\prod_{j=1}^6 \phi_j(\omega_j)$  is bounded by 1 and since it integrates to 0 of periods of length  $2\pi$  its primitive  $\partial^{-1}[\prod_{j=1}^6 \phi_j(\omega_j)]$  is bounded by  $\pi$ .

We use this estimate in each of the terms of the fifth order, all of which have an odd number of sine functions. We estimate all factors  $n_j^2 - x$  by  $N^2$ . Counting the terms and referring to the abbreviations in (12), we obtain 6 terms with a factor  $d$ , 30 factors with a product  $bc$  and 20 terms with a factor  $b^3$ . Thus this term is estimated by

$$(13) \quad \left( \frac{6}{48} + \frac{30}{16} + \frac{20}{8} \right) (1 + \pi) \frac{N^6}{T^5} \leq 19 \frac{N^6}{T^5}.$$

To estimate sixth order terms we estimate all sine and cosine functions by 1. Integrating  $z^{-6}$  then simply gives  $T^{-5}/5$ . We obtain 6 terms with a factor  $R$ , 30 terms with a factor  $bd$ , 15 terms with a factor  $c^2$ , 60 terms with a factor  $cb^2$ , 15 terms with a factor  $b^4$ . This gives the estimate

$$(14) \quad \left( 6 \times 0.0043 + \frac{30}{96} + \frac{15}{64} + \frac{60}{32} + \frac{15}{16} \right) \frac{N^8}{5T^5} \leq 0.68 \frac{N^8}{T^5}.$$

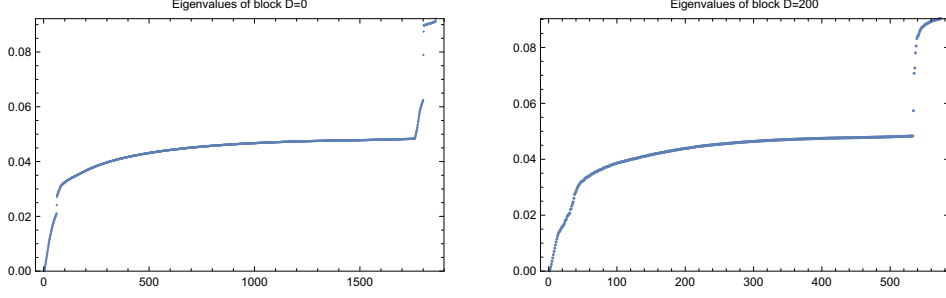
The seventh order terms we estimate similarly. We obtain 30 terms with a factor  $Rb$ , 30 terms with a factor  $dc$ , 60 terms with a factor  $db^2$ , 60 terms with a factor  $c^2b$ , 60 terms with a factor  $cb^3$  and 6 terms with a factor  $b^5$ . This gives the estimate

$$(15) \quad \left( \frac{30}{2} \times 0.0043 + \frac{30}{384} + \frac{60}{192} + \frac{60}{128} + \frac{60}{64} + \frac{6}{32} \right) \frac{N^{10}}{6T^6} \leq 0.35 \frac{N^{10}}{T^6}.$$

Counting the eighth order terms we find 30 terms with a factor  $Rc$ , 60 terms with a factor  $Rb^2$ , 15 terms with a factor  $d^2$ , 120 terms with a factor  $dcb$ , 60 terms with a factor  $db^3$ , 15 terms with a factor  $c^3$ , 45 terms with a factor  $c^2b^2$ , 30 terms with a factor  $cb^4$ , and one term with a factor  $b^6$ . This gives the estimate

$$(16) \quad \begin{aligned} & \left( 0.0043 \left( \frac{30}{8} + \frac{60}{4} \right) + \frac{15}{2304} + \frac{120}{768} + \frac{60}{384} + \frac{15}{512} + \frac{45}{256} + \frac{30}{128} + \frac{1}{32} \right) \frac{N^{12}}{7T^7} \\ & \leq 0.13 \frac{N^{12}}{T^7}. \end{aligned}$$

The terms of order 9 or higher we estimate more crudely. There are at most  $5^6$  terms, the product of prefactors being at most 0.0043 if a factor  $R$

FIGURE 3. Eigenvalues of 1 with  $D = 0, 200$  and  $N = 120$ .

is involved and being at most  $\frac{1}{128}$  if no such factor is involved. Thus we get, assuming  $N^2 \leq T$ , the upper bound

$$(17) \quad \leq \frac{5^6}{128} \frac{N^{14}}{8T^8} \leq 16 \frac{N^{14}}{T^8}.$$

Assuming  $N = 120 \geq 20$  and  $T \geq 10N^2$  we may add (13), (14), (15), (16), and (17) to

$$(18) \quad \begin{aligned} & |I_{\mathbf{k}}^{T,\infty} - \tilde{I}_{\mathbf{k}}^{T,\infty}| \\ & \leq (19 \times 10^{-4} 20^{-2} + 0.68 \times 10^{-4} + 0.35 \times 10^{-5} + 0.13 \times 10^{-6} + 16 \times 10^{-7}) T^{-1} \\ & \leq 0.75 \times 10^{-4} T^{-1} \leq 0.5 \times 10^{-9}. \end{aligned}$$

Here we used  $T = 150,000 > 10N^2$  in the last inequality.

Summing (6), (9), and (18), we obtain

$$(19) \quad |I_{\mathbf{k}} - \tilde{I}_{\mathbf{k}}| \leq 0.73 \times 10^{-9}.$$

### 3. NUMERICAL RESULTS

Using the approximations  $\tilde{I}_{\mathbf{k}}$ , one computes approximations  $(\tilde{Q}_{\mathbf{m},\mathbf{n}})_{\mathbf{m},\mathbf{n} \in X_D}$  to the matrices  $(Q_{\mathbf{m},\mathbf{n}})_{\mathbf{m},\mathbf{n} \in X_D}$  analogously to the formulae in the introduction. Using evaluations of Bessel functions of sufficient accuracy and arbitrary-precision arithmetic, the  $\tilde{I}_{\mathbf{k}}$  and  $\tilde{Q}_{\mathbf{m},\mathbf{n}}$  as well as the eigenvalues of the matrices  $(\tilde{Q}_{\mathbf{m},\mathbf{n}})_{\mathbf{m},\mathbf{n} \in X_D}$  were computed up to an error of at most  $10^{-20}$ . The computed smallest eigenvalue for each  $D$  is plotted in Figure 1 and shown in Table 3 for small  $D$ . In particular, the matrix  $(\tilde{Q}_{\mathbf{m},\mathbf{n}})_{\mathbf{m},\mathbf{n} \in X_D}$  is positive definite with smallest eigenvalue at least 0.000036.

We have for each  $\mathbf{m}, \mathbf{n}$  in question from (19)

$$|Q_{\mathbf{m},\mathbf{n}} - \tilde{Q}_{\mathbf{m},\mathbf{n}}| \leq 16 \times 0.73 \times 10^{-9} \leq 1.2 \times 10^{-8}.$$

This entry-wise bound is multiplied by the size 1860 of the set  $X_D$  for  $N = 120$  to obtain a bound for the operator norm

$$\|(Q_{\mathbf{m},\mathbf{n}})_{\mathbf{m},\mathbf{n} \in X_D} - (\tilde{Q}_{\mathbf{m},\mathbf{n}})_{\mathbf{m},\mathbf{n} \in X_D}\|_{op} \leq 1860 \times 1.2 \times 10^{-8} \leq 0.000023.$$

As this is less than the smallest eigenvalue of the matrix

$$(\tilde{Q}_{\mathbf{m},\mathbf{n}})_{\mathbf{m},\mathbf{n} \in X_D},$$

$D$	$\lambda_{\min}$
0	0.0000362610
2	0.0000364272
4	0.0000367725
6	0.0000372058
8	0.0000377326
10	0.0000383058

TABLE 1. Smallest eigenvalues for matrices  $(Q_{\mathbf{m},\mathbf{n}})_{\mathbf{m},\mathbf{n} \in X_D}$ , for  $D = 0, 2, \dots, 10$ , rounded to 11 significant figures.

we may deduce that the matrix  $(Q_{\mathbf{m},\mathbf{n}})_{\mathbf{m},\mathbf{n} \in X_D}$  is positive definite as well. Following the reductions of [OTZ19], this proves Theorem 1.

While the error bounds (19) are good enough to prove the main theorem, they are not good enough to guarantee that our plots and tables of eigenvalues of  $(\tilde{Q}_{\mathbf{m},\mathbf{n}})_{\mathbf{m},\mathbf{n} \in X_D}$  are representative for those of  $(Q_{\mathbf{m},\mathbf{n}})_{\mathbf{m},\mathbf{n} \in X_D}$  within the margins suggested by the visible information. However, the arguments obtaining (19) as well as the use of the operator norm above are very crude estimates. With very high likelihood, the true differences between the corresponding eigenvalues of the two matrices are much smaller than the operator norm above. In this sense, we consider our plots and tables of eigenvalues of  $(\tilde{Q}_{\mathbf{m},\mathbf{n}})_{\mathbf{m},\mathbf{n} \in X_D}$  as very much representative of those of  $(Q_{\mathbf{m},\mathbf{n}})_{\mathbf{m},\mathbf{n} \in X_D}$ . This is in accordance with the rather regular behaviour of the plots and of Table 3, a level of regularity that one might expect from the eigenvalues of  $(Q_{\mathbf{m},\mathbf{n}})_{\mathbf{m},\mathbf{n} \in X_D}$ .

A number of numerical findings would be interesting to understand analytically and maybe prove for large  $N$  asymptotically. Any progress in this understanding would presumably require an asymptotic understanding of the entries of the matrices in (1). Figure 4 shows sample columns of these matrices. For nicer visualization, we have undone the dimension reduction by symmetry in [OTZ19] and shown the related matrices

$$(20) \quad \tilde{Q}^{(D)} := (Q_{\mathbf{m},\mathbf{n}})_{\mathbf{m},\mathbf{n} \in Z_D},$$

in the space

$$Z_D := \left\{ (m_1, m_2, m_3) \in (2\mathbb{Z})^3 \setminus \{(0,0,0)\} \mid \begin{array}{l} m_1+m_2+m_3=D, \\ |m_1|, |m_2|, |m_3| \leq N \end{array} \right\}.$$

The space  $Z_D$  is naturally depicted as a hexagon. It has a sixfold symmetry under permutations of the three elements, which is the symmetry group of a regular hexagon. This symmetry extends to symmetries of the columns shown and is visible in the plots of Figure 4. The space  $X_D$  in our previous calculations is only one fundamental domain under this symmetry.

The largest entry in each column of the matrices in (1) is the diagonal element. The diagonal elements are shown as red dots in Figure 4. Due to the sixfold symmetry of the visualization, they appear three or six times in each image depending on their orbit under the symmetry group, namely the points where  $\mathbf{m}$  is a permutation of  $\mathbf{n}$ . While it may be tempting to try to prove positive definiteness of the matrices in (1) by diagonal dominance, for

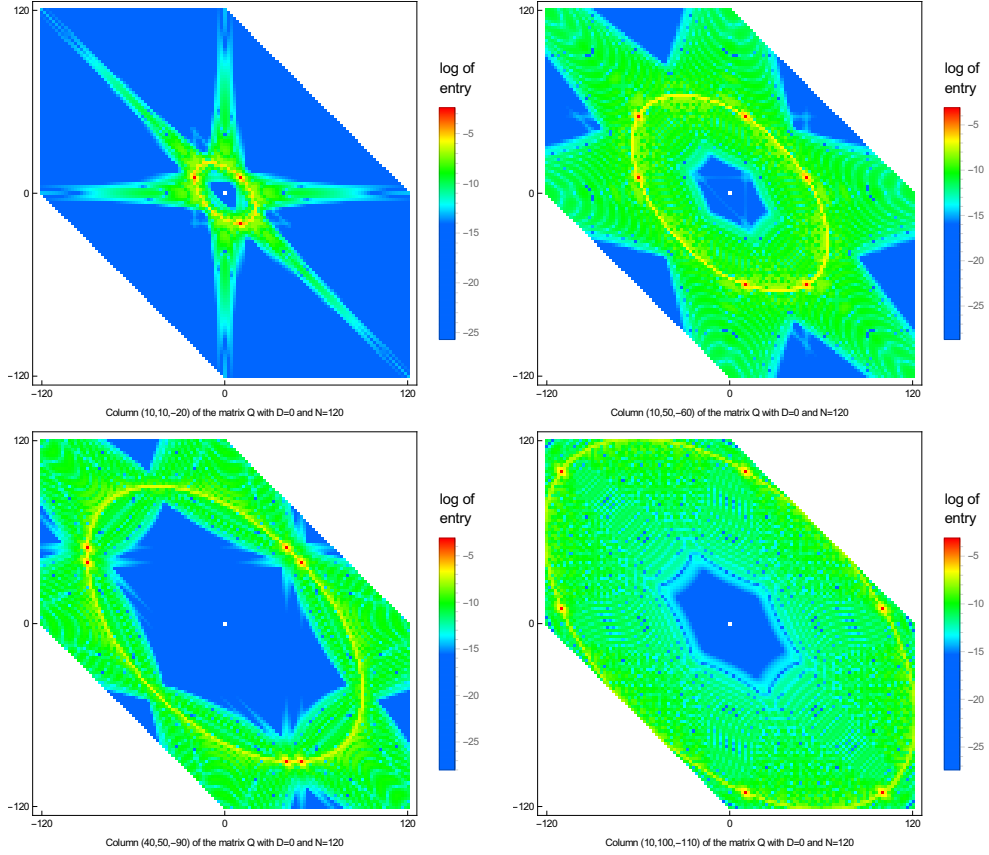


FIGURE 4. Columns of (20) with  $D = 0$ ,  $N = 120$ , and  $\mathbf{m}$  fixed, in coordinates  $n_1, n_2$ , colored logarithmically according to absolute values of entries.

$N = 120$  and  $D = 0$ , the ratios

$$(21) \quad r_{\mathbf{m}} := |Q_{\mathbf{m},\mathbf{m}}|^{-1} \sum_{\mathbf{n} \in X_0 \setminus \{\mathbf{m}\}} |Q_{\mathbf{m},\mathbf{n}}|,$$

can be large as well as small, e.g.

$$r_{(-2,0,2)} \approx 3.1, \quad r_{(-90,40,50)} \approx 1.9, \quad r_{(-4,2,2)} \approx 0.7.$$

Indeed, this failure of this attempt is natural due to the existence of some very small eigenvalues.

A secondary collection of large entries in each column shown in Figure 4 can be seen as yellow ellipses in the diagrams. These visual ellipses correspond to circles in a visualization of the domain as regular hexagon. The circles were already observed in [OTZ19]. 21. The current data even more strongly suggests that these secondary peaks are located on the surface

$$(22) \quad n_1^2 + n_2^2 + n_3^2 = m_1^2 + m_2^2 + m_3^2.$$

Indeed, in Figure 5, the ellipse/circle given by (22) shown as dashed grey line is overlaid onto one of the plots, showing that it matches the yellow peaks

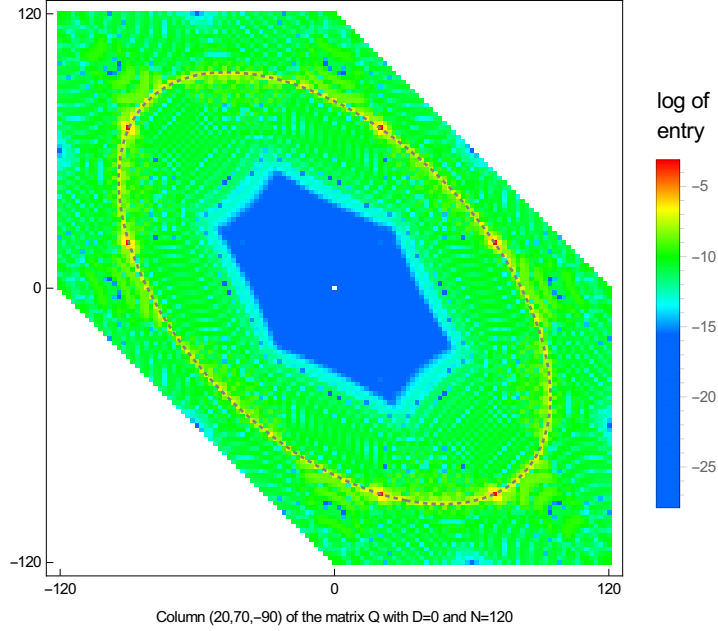


FIGURE 5. Column  $\mathbf{m} = (20, 70, -90)$  of (20) with  $D = 0$  and  $N = 120$ , in coordinates  $n_1, n_2$ , with the ellipse given by (22).

very well. The size of the sum of off-diagonal elements in (21) is essentially entirely due to the elements near the circle.

At the moment, we do not even have a qualitative understanding of the occurrence of these circles, let alone a quantitative one, which would probably be required if one wanted to extract positive definiteness from the structure of these matrices. Figure 6 plots the values of the entries of the column  $(40, 60, -100)$  as a function of the radial variable  $\sqrt{n_1^2 + n_2^2 + n_3^2}$  in the vicinity of the radius of the yellow circle, which is about 123.3. The plot strongly suggests that the pattern of the circle is asymptotically well approximated by a smooth radial function of low complexity. The value at the diagonal element, which is at radius about 123.3, is not plotted in Figure 6, because it is too large at about 0.044. Likewise, two further entries near the diagonal elements are not shown, they have value  $-0.0024$ . They are part of the small ring of six large elements around the diagonal elements, which also include the four entries with values near  $-0.0015$  shown in Figure 6. Also, small matrix entries are cut off in the plot 6.

Due to the monotonicity shown in Figure 1, it is of particular interest to study the matrix in (1) for  $D = 0$ . Figure 3 shows all eigenvalues of the matrix  $D = 0$  for  $N = 120$  sorted and enumerated by size. For comparison, we also show the analogous plot for the matrix  $D = 200$ , a diagram that is somewhat similar. Note the two jumps of the diagram for  $D = 0$  at about the 60-th smallest and 60-th largest eigenvalues. An analytical proof of positivity for all  $N$  in the asymptotic regime would require a better understanding of the ensemble of small eigenvalues below the first jump.

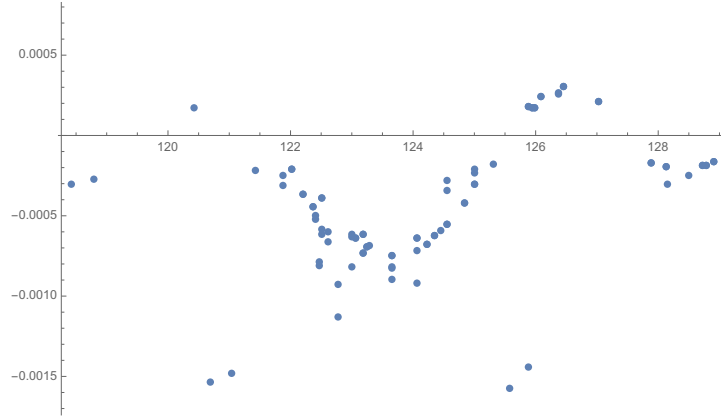


FIGURE 6. Partial plot of the values of the entries of column  $\mathbf{m} = (40, 60, -100)$  of (20) with  $D = 0$  and  $N = 120$  in dependence of the radial variable.

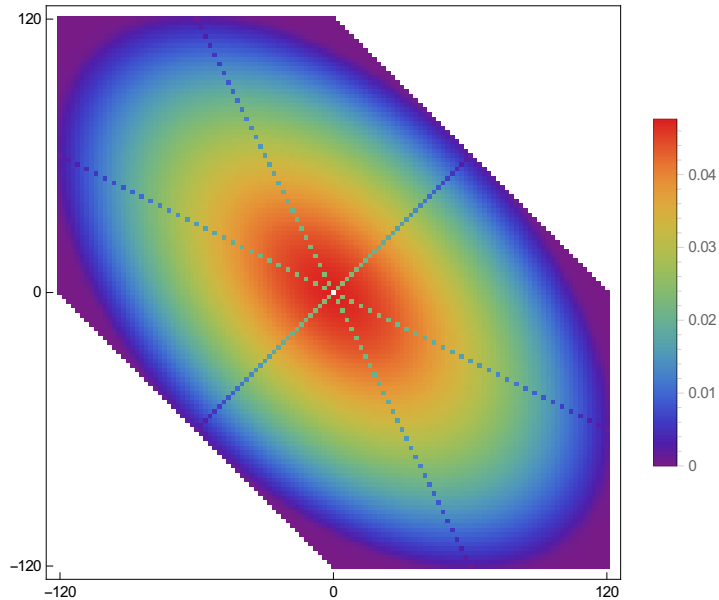


FIGURE 7. Eigenvector of (20) corresponding to the smallest eigenvalue in coordinates  $n_1, n_2$ . The dotted lines are an artifact of the representation, they describe the points where the orbit of the symmetry group has only three elements.

The eigenfunctions corresponding to the smallest eigenvalues experimentally appear to be essentially radial functions in the visualization corresponding to Figure 4, see Figure 7. There are three notable observations to be made here.

- (1) The bulk of the eigenvector depends essentially only on  $\sqrt{n_1^2 + n_2^2 + n_3^2}$ .
- (2) The value at the points where two of the  $n_i$ 's coincide is smaller than suggested by this radial dependence by a factor 2 (although this is not evident from this particular visualization).



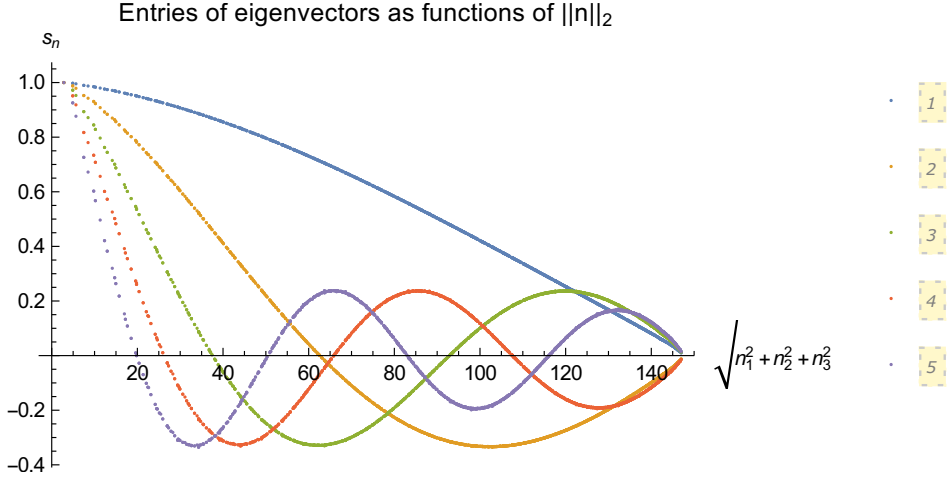


FIGURE 8. Eigenfunctions associated to 5 smallest eigenvalues of (23) with  $D = 0$  and  $N = 120$ . Each color represents one eigenvector  $(s_{\mathbf{n}})$  and each point one entry of this eigenvector. The horizontal axis shows  $\sqrt{n_1^2 + n_2^2 + n_3^2}$  and the vertical axis  $s_{\mathbf{n}}$ .

- (3) Outside of the largest circle that fits into the region  $Z_0$ , the eigenvector is small.

The second point above is related to the fact that in the matrices (20), the rows and the columns of (20) appear as many times as there are distinct permutations of  $\mathbf{m}$  and  $\mathbf{n}$ , respectively, which can be either 3 or 6 times. It therefore appears more natural to analyze the eigenvalues of (20), or, equivalently, the matrices given by  $(p_{\mathbf{m}}Q_{\mathbf{m},\mathbf{n}}p_{\mathbf{n}})_{\mathbf{m},\mathbf{n} \in X_0}$ , where  $p_{\mathbf{m}}$  is the number of distinct permutations of  $\mathbf{m}$ .

In view of the third point above, it also appears natural to truncate the matrices not according to  $\max(|n_1|, |n_2|, |n_3|)$ , but according to  $\sqrt{n_1^2 + n_2^2 + n_3^2}$ . In what follows, let us therefore consider the matrices

$$(23) \quad Q^\circ := (p_{\mathbf{m}}Q_{\mathbf{m},\mathbf{n}}p_{\mathbf{n}})_{\mathbf{m},\mathbf{n} \in X^\circ},$$

where

$$X^\circ = \left\{ (m_1, m_2, m_3) \in (2\mathbb{Z})^3 \setminus \{(0,0,0)\} \mid \begin{array}{l} m_1 + m_2 + m_3 = 0, \\ \sqrt{m_1^2 + m_2^2 + m_3^2} \leq \sqrt{3/2}N, \\ m_1 \leq m_2 \leq m_3 \end{array} \right\}.$$

is the largest disc contained in  $X_0$ .

The eigenvectors of the matrices (23) corresponding to small eigenvalues seem to be smooth functions of the radial variable  $\sqrt{n_1^2 + n_2^2 + n_3^2}$ , see Figure 8. That figure does not show sections of two-dimensional functions; it rather contains a point for each  $\mathbf{n} \in X^\circ$  on every curve. The profile of these eigenvectors seems to be independent of  $N$  in the asymptotic regime, as shown in Figure 9.

It is natural to link the behaviour of the eigenfunctions to the smallest eigenvectors to a natural enemy of the sharp Fourier extension conjecture. Namely, functions on the circle which approximate two Dirac deltas at antipodally symmetric points are close competitors to extremize the

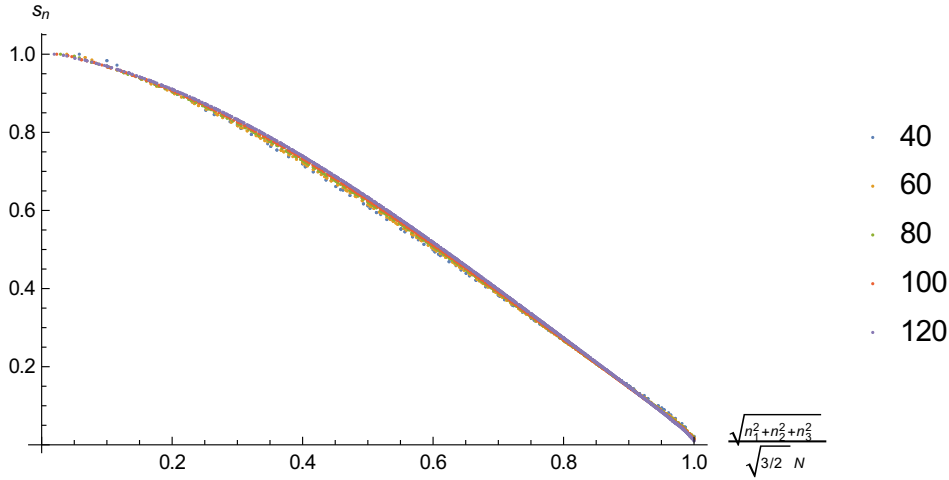


FIGURE 9. Eigenfunctions associated to the smallest eigenvalues of (23) with  $D = 0$  and  $N \in \{40, 60, 80, 100, 120\}$ . Each color represents one value of  $N$  and each point one entry of the corresponding eigenvector. The horizontal axis shows  $\sqrt{n_1^2 + n_2^2 + n_3^2}/(\sqrt{3/2}N)$  and the vertical axis  $s_{\mathbf{n}}$ .

Tomas-Stein functional; they “lose” to the constant function by only a small amount. Such Dirac deltas, on the Fourier transform side depicted in the above hexagons, correspond to wide bumps such as the lowest eigenfunction. One can well imagine that all the radial eigenfunctions to small eigenvalues aspire to resolve structure near the Dirac deltas.

#### ACKNOWLEDGEMENTS

The main calculations were performed using the supercomputing facilities of Fraunhofer SCAI. The authors acknowledge support by the Hausdorff Center for Mathematics and the Deutsche Forschungsgemeinschaft through the Collaborative Research Center 1060.

#### REFERENCES

- [Car+17] Emanuel Carneiro et al. *A sharp trilinear inequality related to Fourier restriction on the circle*. In: *Rev. Mat. Iberoam.* 33.4 (2017), pp. 1463–1486. ISSN: 0213-2230. DOI: 10.4171/RMI/978. URL: <https://doi.org/10.4171/RMI/978>.
- [FO17] Damiano Foschi and Diogo Oliveira e Silva. *Some recent progress on sharp Fourier restriction theory*. In: *Anal. Math.* 43.2 (2017), pp. 241–265. ISSN: 0133-3852. DOI: 10.1007/s10476-017-0306-2. URL: <https://doi.org/10.1007/s10476-017-0306-2>.
- [Joh17] Fredrik Johansson. *Arb: efficient arbitrary-precision midpoint-radius interval arithmetic*. In: *IEEE Transactions on Computers* 66.8 (2017), pp. 1281–1292.
- [OT15] Diogo Oliveira e Silva and Christoph Thiele. *Estimates for certain integrals of products of six Bessel functions*. In: *Rev. Mat. Iberoam* (2015).

- [OTZ19] Diogo Oliveira e Silva, Christoph Thiele, and Pavel Zorin-Kranich. *Band-limited maximizers for a Fourier extension inequality on the circle*. In: *Experimental Mathematics* (2019), pp. 1–7.
- [Tom75] Peter A. Tomas. *A restriction theorem for the Fourier transform*. In: *Bull. Amer. Math. Soc* 81.2 (1975), pp. 477–478.
- [W19] Wolfram Research, Inc. *Mathematica, Version 12.0*. Champaign, IL, 2019. URL: <https://www.wolfram.com/mathematica>.

(Barker) FRAUNHOFER SCAI, SCHLOSS BIRLINGHOVEN, 53754 SANKT AUGUSTIN, GERMANY

*E-mail address:* `james.barker@scai.fraunhofer.de`

(Barker) INSTITÜT FÜR NUMERISCHE SIMULATION, ENDENICHER ALLEE 19B, 53115 BONN, GERMANY

(Thiele, Zorin-Kranich) HAUSDORFF CENTER FOR MATHEMATICS, 53115 BONN, GERMANY

*E-mail address:* `thiele@math.uni-bonn.de`

*E-mail address:* `pzorin@math.uni-bonn.de`